PHYSICAL REVIEW E **94**, 050101(R) (2016)

Eigenvalue spectra of large correlated random matrices

Alexander Kuczala and Tatyana O. Sharpee
Computational Neurobiology Laboratory, Salk Institute for Biological Studies, La Jolla, California 92037, USA
and Department of Physics, University of California, San Diego, California 92161, USA
(Received 4 July 2016; revised manuscript received 4 October 2016; published 17 November 2016)

Using the diagrammatic method, we derive a set of self-consistent equations that describe eigenvalue distributions of large correlated asymmetric random matrices. The matrix elements can have different variances and be correlated with each other. The analytical results are confirmed by numerical simulations. The results have implications for the dynamics of neural and other biological networks where plasticity induces correlations in the connection strengths within the network. We find that the presence of correlations can have a major impact on network stability.

DOI: 10.1103/PhysRevE.94.050101

Random matrices serve as a useful tool for analyzing the stability and dynamics of a variety of networks, from neuroscience [1–4] and genetic circuits [5] to ecology [6,7]. Spectra of random matrices also help determine solutions to problems in nuclear [8] and condensed matter physics [9,10] as well as in data compression [11,12]. In particular, the rightmost eigenvalue (the eigenvalue with largest real component) determines the stability of the system's linear dynamics and the onset of chaos of the nonlinear dynamics. Knowledge of the onset of chaos is useful for determining the network's computational capabilities [13,14] as well as the network's response to inputs [15].

However, most of these results do not address an important feature of biological circuits where connection strengths are correlated [16–18]. While correlated Hermitian ensembles have received some attention, [19–22], results about correlated non-Hermitian ensembles are scarce [23,24]. Most notably, the correlations in the connection strengths arise as the result of plasticity, where connections are modified depending on node activity and network input. One of the predominant effects of plasticity is that it induces correlations between forward and reverse connections [16,18]. That is, the degree to which node i affects node j is correlated with the strength of the reverse connection from node j to node i. We focus here on this circuit motif when considering correlations between matrix elements.

Consider a network with N nodes $i = 1, \ldots, N$, with linear dynamics

$$\dot{x}_i(t) = -x_i(t) + \sum_{j=1}^{N} J_{ij} x_j(t), \tag{1}$$

where $x_i(t)$ describes the activity of each node and J is the $N \times N$ connectivity matrix. The solution of this system is $\mathbf{x}(t) = e^{(\mathbf{1}-\mathbf{J})t}\mathbf{x}(0)$. This system has stable equilibria only if the rightmost eigenvalue of J is less than one. For networks with nonlinear dynamics, mean-field methods can be used to show that the transition to chaotic behavior still occurs when the rightmost eigenvalue of J is $=1$ [1,3,4].

In this Rapid Communication we use the diagrammatic approach to analyze the case where the matrix elements of J are correlated and not identically distributed. Specifically, we consider an $N \times N$ complex non-Hermitian Gaussian random matrix J whose elements are distributed according to

$$P(J) \propto \exp\left[-\frac{N}{2}\sum_{i,j}\begin{pmatrix} J_{ij}^* & J_{ji}^* \end{pmatrix}\mathbf{V}^{-1}\begin{pmatrix} J_{ij} \\ J_{ji} \end{pmatrix}\right], \tag{2}$$

where covariance matrix $\mathbf{V}$ consists of real-valued variances

$$\langle J_{ij} J_{ij}^* \rangle = \frac{1}{N} g_{ij}^2, \tag{3}$$

and real-valued covariances

$$\langle J_{ij} J_{ji} \rangle = \frac{1}{N} \tau_{ij} g_{ij} g_{ji}. \tag{4}$$

All other second-order correlations vanish. The gain matrix g_{ij} has positive elements. Correlation values τ_{ij} are symmetric in i, j, $|\tau_{ij}| \leqslant 1$, and denote the degree of correlation between forward j,i and reverse i,j connections in the corresponding random network.

To outline the steps of the derivation, we first seek the expected density of eigenvalues of J for large N by first writing the density in terms of the Green's function G. While G is analytic for Hermitian matrices, G is generally nonanalytic for non-Hermitian matrices, so we cannot directly apply the diagrammatic method. We therefore relate G to the analytic Green's function of a Hermitian random matrix H, which we compute with standard diagrammatic techniques. We derive a set of self-consistent equations for G for the case where the gain matrix g_{ij} is a continuous function in the limit $N \to \infty$, and the case where g_{ij} is block structured. Finally, we apply our method to two example problems and compare the results to empirical eigenvalue distributions obtained by exact diagonalization of realizations of J.

We start by writing the expected density of eigenvalues of J in the complex plane as

$$\rho(x,y) = \left\langle \frac{1}{N}\sum_k \delta(x - \operatorname{Re}\lambda_k)\delta(y - \operatorname{Im}\lambda_k) \right\rangle. \tag{5}$$

where $\langle\cdot\rangle$ indicates an average over realizations of J according to Eq. (2). Defining $\partial = (\partial_x - i\partial_y)/2$ and $\bar{\partial} = (\partial_x + i\partial_y)/2$, and using the identity $\bar{\partial}\frac{1}{x+iy} = \pi\delta(x)\delta(y)$ [25], we can write the density (5) in terms of the Green's function

$$G(z,\bar{z}) \equiv \left\langle \frac{1}{N}\operatorname{tr}\frac{1}{z - J} \right\rangle \tag{6}$$

as

$$\rho(x,y) = \frac{1}{\pi}\bar{\partial}G(z,\bar{z}). \tag{7}$$

Since J is non-Hermitian, the eigenvalues of J will in general lie in some region of the complex plane. For example, Ginibre's circular law states that if the elements of J are independently and identically distributed with variances g^2/N, then the eigenvalues lie in a disk of radius g [26]. The Green's function is therefore not in general holomorphic, and we cannot expand in powers of $1/z$ as required for the diagrammatic expansion. Following Ref. [27], we can find the Green's function by solving a related Hermitian random matrix problem, to which we can apply the diagrammatic approach. Define the $2N \times 2N$ Hermitian matrix

$$H = \begin{bmatrix} 0 & J-z \\ (J-z)^\dagger & 0 \end{bmatrix}. \tag{8}$$

The matrix Green's function for H is

$$\mathcal{G}(\eta,z,\bar{z}) = \left\langle \frac{1}{\eta - H} \right\rangle, \tag{9}$$

where we think of the eigenvalues of H as lying on the complex plane η. Since H is Hermitian, these eigenvalues will lie on the real axis, and $\mathcal{G}$ is holomorphic in η except for cuts on the real axis. Once $\mathcal{G}$ is computed, we obtain the original Green's function G from $\mathcal{G}$ by extracting the lower left matrix block and taking the limit $\eta \to i0^+$,

$$\mathcal{G}(\eta = 0,z,\bar{z}) = \left\langle \begin{bmatrix} 0 & \frac{1}{(z-J)^\dagger} \\ \frac{1}{z-J} & 0 \end{bmatrix} \right\rangle, \tag{10}$$

yielding Eq. (6):

$$G(z,\bar{z}) = \frac{1}{N}\mathrm{tr}\,\mathcal{G}^{21}(\eta = 0,z,\bar{z}). \tag{11}$$

Here, $\mathcal{G}^{21}$ is the lower left block of $\mathcal{G}$. To compute $\mathcal{G}$ (9), we first rewrite $\eta - H = \mathcal{G}_0^{-1} - \mathcal{J}$ with

$$\mathcal{G}_0^{-1} \equiv \begin{bmatrix} \eta & z \\ \bar{z} & \eta \end{bmatrix} \quad \text{and} \quad \mathcal{J} \equiv \begin{bmatrix} 0 & J \\ J^\dagger & 0 \end{bmatrix}, \tag{12}$$

so that the random part $\mathcal{J}$ has zero mean. Note that $\mathcal{G}_0$ is just $\mathcal{G}$ with $J = 0$. We expand $\mathcal{G}$ in $\mathcal{G}_0$ as follows:

$$\mathcal{G} = \sum_{n=0}^{\infty} \mathcal{G}_0\langle(\mathcal{J}\mathcal{G}_0)^n\rangle = \mathcal{G}_0 + \langle\mathcal{G}_0\mathcal{J}\mathcal{G}_0\mathcal{J}\mathcal{G}_0\rangle + \cdots. \tag{13}$$

Here, the odd terms vanish since $\langle\mathcal{J}\rangle = 0$. Since the distribution over $\mathcal{J}$ is Gaussian, each term in the sum reduces to the Wick contraction of n factors of $\mathcal{J}$. We therefore use the diagrammatic technique [28,29] to represent each term in the sum. We denote the N node indices by roman letters $i,j = 1,\ldots,N$ and index the blocks by greek letters $\alpha,\beta = 1,2$. We represent $\mathcal{G}_0$ by a single directed line carrying one set of indices, and the correlator $\langle\mathcal{J}\mathcal{J}\rangle$ by a double line carrying two sets of indices (Fig. 1) [27,30,31]. Indices are summed at each connecting vertex. The nth term in $\mathcal{G}$ is the sum of all diagrams with n vertices. In the large N limit diagrams which have crossing lines vanish, and only "planar" diagrams remain [32–34]. This greatly simplifies the sum, since the only allowed diagrams are nested "rainbow diagrams" such as

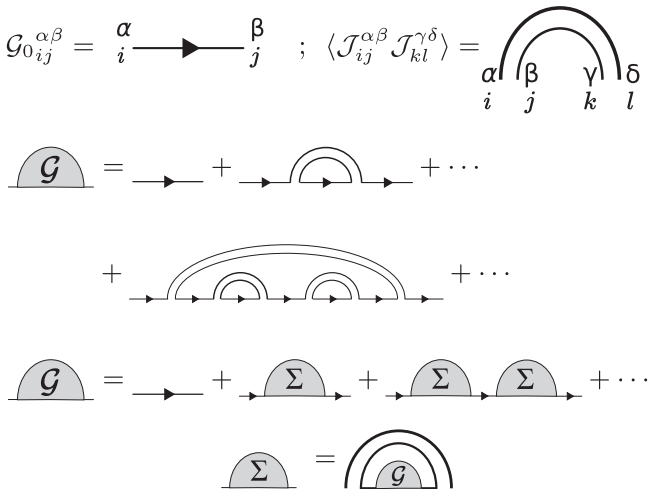

FIG. 1. Diagrams used in the expansion (13) of $\mathcal{G}$. $\mathcal{G}$ is the sum of all planar diagrams in the large N limit. $\mathcal{G}$ can be resummed in terms of the self-energy matrix Σ. In the large N limit, Σ consists of all diagrams nested under a double line (15).

those depicted in Fig. 1. This allows us to evaluate (13) by performing a resummation of $\mathcal{G}$ in terms of the "self-energy" matrix Σ:

$$\mathcal{G} = \sum_{n=0}^{\infty} \mathcal{G}_0(\Sigma\mathcal{G}_0)^n = \left(\frac{1}{\mathcal{G}_0^{-1} - \Sigma}\right). \tag{14}$$

In the planar limit, the self-energy matrix is

$$\Sigma = \langle\mathcal{J}\mathcal{G}\mathcal{J}\rangle, \tag{15}$$

encoding the nested "rainbow" structure of the diagrams [29]. This is depicted diagrammatically in Fig. 1.

In block form, Eq. (14) is

$$\mathcal{G} = \begin{bmatrix} A & B \\ C & D \end{bmatrix} = \begin{bmatrix} \eta - \Sigma^{11} & z - \Sigma^{12} \\ \bar{z} - \Sigma^{21} & \eta - \Sigma^{22} \end{bmatrix}^{-1}, \tag{16}$$

and Eq. (15) is

$$\Sigma = \begin{bmatrix} \Sigma^{11} & \Sigma^{12} \\ \Sigma^{21} & \Sigma^{22} \end{bmatrix} = \left\langle \begin{bmatrix} JDJ^\dagger & JCJ \\ J^\dagger BJ^\dagger & J^\dagger AJ \end{bmatrix} \right\rangle, \tag{17}$$

where we have denoted the blocks of $\mathcal{G}$ as A, B, C, and D. Substituting (17) into (16) will give us self-consistent equations for the blocks of $\mathcal{G}$.

Equations (16) and (17) describe the eigenvalue distribution in the general case, with or without correlations. Before analyzing the impact of correlations on the eigenvalue distribution, we first check that this result reproduces previous results obtained in the absence of correlations. When elements of J are independently distributed, the covariances (4) vanish. In this case we find [35]

$$\Sigma_{il}^{11} = \sum_{j,k}\langle J_{ij}D_{jk}J_{kl}^\dagger\rangle = \frac{1}{N}\delta_{il}\sum_j g_{ij}g_{lj}D_{jj}, \tag{18}$$

$$\Sigma_{il}^{22} = \sum_{j,k}\langle J_{ij}^\dagger A_{jk}J_{kl}\rangle = \frac{1}{N}\delta_{il}\sum_j g_{ji}g_{jl}A_{jj}, \tag{19}$$

and $\Sigma^{12} = \Sigma^{21} = 0$. This means that the matrix Σ is diagonal. Then, since each block on the right-hand side (RHS) of Eq. (16) is diagonal, each block of $\mathcal{G}$ is also diagonal. Inverting the RHS and equating matrix elements yields

$$A_{ii} = \frac{\eta - \frac{1}{N}\sum_j A_{jj} g_{ji}^2}{q_i(\eta,|z|)}, \quad D_{ii} = \frac{\eta - \frac{1}{N}\sum_j g_{ij}^2 D_{jj}}{q_i(\eta,|z|)}, \tag{20}$$

$$C_{ii} = \bar{z}/q_i(\eta,|z|), \tag{21}$$

where

$$q_i(\eta,|z|) = \left(\eta - \frac{1}{N}\sum_j A_{jj} g_{ji}^2\right)\left(\eta - \frac{1}{N}\sum_j g_{ij}^2 D_{jj}\right) - |z|^2. \tag{22}$$

Writing out the blocks of $\mathcal{G}$ in Eq. (9),

$$\begin{bmatrix} A & B \\ C & D \end{bmatrix} = \left\langle \begin{bmatrix} \frac{\eta}{\eta^2-(J-z)(J-z)^\dagger} & \frac{J-z}{\eta^2-(J-z)^\dagger(J-z)} \\ \frac{(J-z)^\dagger}{\eta^2-(J-z)(J-z)^\dagger} & \frac{\eta}{\eta^2-(J-z)^\dagger(J-z)} \end{bmatrix} \right\rangle, \tag{23}$$

and rewriting $\eta = i\epsilon$, with $\epsilon > 0$, we see that blocks A and D are positive definite matrices multiplied by $-i$. We therefore define $a_j \equiv iA_{jj}$ and $d_j \equiv iD_{jj}$, where a_i and d_i are positive real numbers. We also define $c_j = C_{jj}$. This allows us to rewrite (20) and (21) as

$$a_i = \hat{a}_i/q_i, \quad d_i = \hat{d}_i/q_i, \quad c_i = \bar{z}/q_i(\epsilon,|z|), \tag{24}$$

with $q_i(\epsilon,r) \equiv -q_i(\eta,|z|) = \hat{a}_i\hat{d}_i + r^2$ and

$$\hat{a}_i \equiv \epsilon + \frac{1}{N}\sum_j a_j g_{ji}^2, \quad \hat{d}_i \equiv \epsilon + \frac{1}{N}\sum_j g_{ij}^2 d_j, \tag{25}$$

where $r = |z|$. We now have a set of $2N$ self-consistent equations (24) for the elements a_i and d_i of the Green's function $\mathcal{G}$. These can be solved numerically with $\epsilon = 0$ (or ϵ set to a small value if many elements g_{ij} are also small). Once the a_i and d_i are found, the c_i can be computed and used to find the original Green's function G with Eq. (11), since the trace of $\mathcal{G}^{21} \equiv C$ is the sum of the coefficients $c_i \equiv C_{ii}$. Note that since $c_j = re^{-i\theta}/q_j(\epsilon,r)$ in polar coordinates, $|c_j|$ depends only on r. This allows us to rewrite Eq. (7) as a function of r only:

$$\rho(r) = \frac{1}{2\pi N}\sum_j \left(\frac{\partial|c_j|}{\partial r} + \frac{|c_j|}{r}\right). \tag{26}$$

The resulting eigenvalue distribution has support on the disk with radius $r = \sqrt{\lambda_1(K)}$, where $\lambda_1(K)$ is the largest eigenvalue of the matrix $K_{ij} \equiv g_{ij}^2/N$ (see the Appendix).

Symmetric covariances. We now allow J to have correlated elements across its diagonal [Eq. (4)]. Then Σ^{12} and $\Sigma^{21} \neq 0$, yielding a new expression for c,

$$c_i = \hat{c}_i/q_i(\epsilon,z,\bar{z}), \quad \hat{c}_i \equiv \bar{z} - \frac{1}{N}\sum_j \tau_{ij} g_{ij} g_{ji} \bar{c}_j, \tag{27}$$

where now $q_i = \hat{a}_i\hat{d}_i + |\hat{c}_i|^2, b_i = \bar{c}_i$. The τ_{ij} denote the degree of correlation between i and j as in Eq. (4). In this case, the eigenvalue density has the more general form

$$\rho(x,y) = \frac{1}{\pi}\partial\bar{\partial}G(z,\bar{z}) = \frac{1}{N\pi}\partial\bar{\partial}\sum_{j=1}^{N} c_j(z,\bar{z}). \tag{28}$$

The density ρ depends on x and y in a nontrivial way, and the support of the distribution is in general neither circular nor elliptical. The boundary of the eigenvalue distribution now satisfies (see the Appendix for a derivation)

$$\lambda_1(K(z)) = 1, \quad K_{ij}(z) = \frac{1}{N}|c_i(z)|^2 g_{ij}^2, \tag{29}$$

where the complex-valued $c_i(z)$ are now given by the self-consistent equations

$$c_i = \left(z - \sum_j \tau_{ij} g_{ij} g_{ji} c_j\right)^{-1}. \tag{30}$$

Now, to obtain the boundary, it is necessary to simultaneously solve (29) and (30) for each boundary point. For example, we can set $z = re^{i\theta}$ and solve the above for r for each θ. Note that these expressions reduce to the circularly symmetric case when $\tau_{ij} = 0$.

Block structured. We now consider the special case for which the gain matrix g_{ij} is block structured. Block structured matrices describe networks with nodes partitioned into subgroups, for example, neural networks with cell-type-specific connectivity [3], or networks of ecological communities [24]. Suppose the nodes of the network are grouped into M populations of size $f_m N$, for $m = 1,\ldots,M$, and that J is block structured so that the gain $g_{m_i n_j}^2 = g_{mn}^2$ and correlations $\tau_{m_i n_j} = \tau_{mn}$ depend only on the population indices m and n of the output and input nodes i and j, respectively. This allows us to sum (24) and (27) over each population. Let $N_m \equiv N\sum_{n=1}^{m} f_n$. Then define [36]

$$a_m \equiv \frac{1}{Nf_m}\sum_{i=N_{m-1}+1}^{N_m} a_i, \tag{31}$$

and define c_m and d_m similarly. Then $q_m \equiv q_i$ depends only on the population index, and now we have

$$a_m = \hat{a}_m/q_m, \quad d_m = \hat{d}_m/q_m, \quad c_m = \hat{c}_m/q_m, \tag{32}$$

and $q_m = \hat{a}_m\hat{d}_m + |\hat{c}_m|^2$, with

$$\hat{a}_m = \epsilon + \sum_{n=1}^{M} f_n a_n g_{nm}^2, \quad \hat{d}_m = \epsilon + \sum_{n=1}^{M} g_{mn}^2 f_n d_n, \tag{33}$$

$$\hat{c}_m = \bar{z} - \sum_{n=1}^{M} \tau_{mn} g_{mn} g_{nm} f_n \bar{c}_n. \tag{34}$$

Now the dependence on N is removed, and we need only solve $3M$ self-consistent equations. The eigenvalue density is now

$$\rho(x,y) = \frac{1}{\pi}\partial\sum_m f_m c_m(z,\bar{z}). \tag{35}$$

The boundary of the distribution satisfies equations similar to (29) and (30) (see the Appendix). When $\tau_{mn} = 0$, the distribution has boundary $|z| = \sqrt{\lambda_1(K)}$, where $\lambda_1(K)$ is the largest eigenvalue of the matrix $K_{mn} \equiv g_{mn}^2 f_n$ [3].

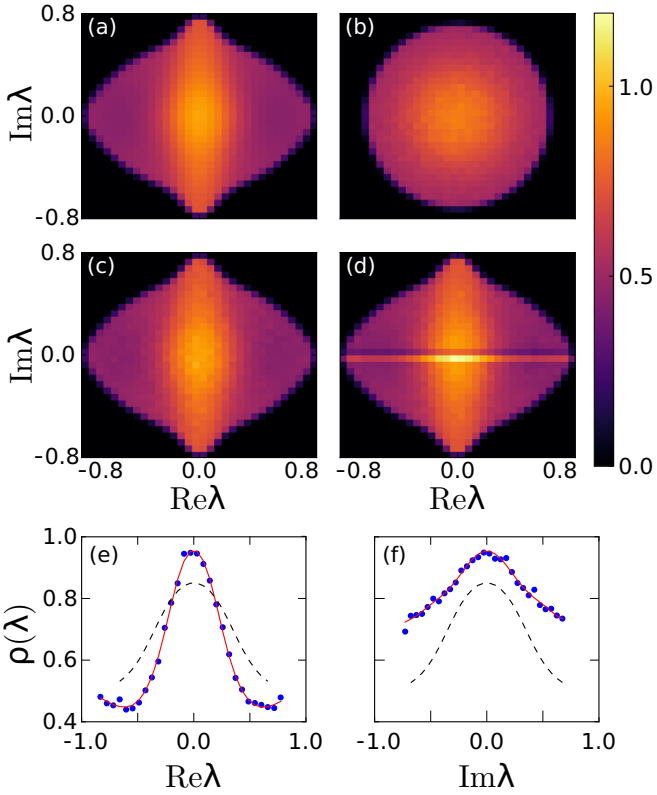

FIG. 2. Eigenvalue density for block structured J with gain and covariance given by (36). (a) Eigenvalue density calculated from self-consistent equations (32). (b) Empirical histogram of eigenvalues from exact diagonalization of realizations of J with independent elements. The empirical histogram for J with covariance is shown with (c) complex and (d) real entries. (e), (f) Cross sections of the density along the (e) real and (f) imaginary axes, showing the theoretical result (solid red line), the complex-valued empirical result (blue dots), and the distribution with no covariance (dashed curve).

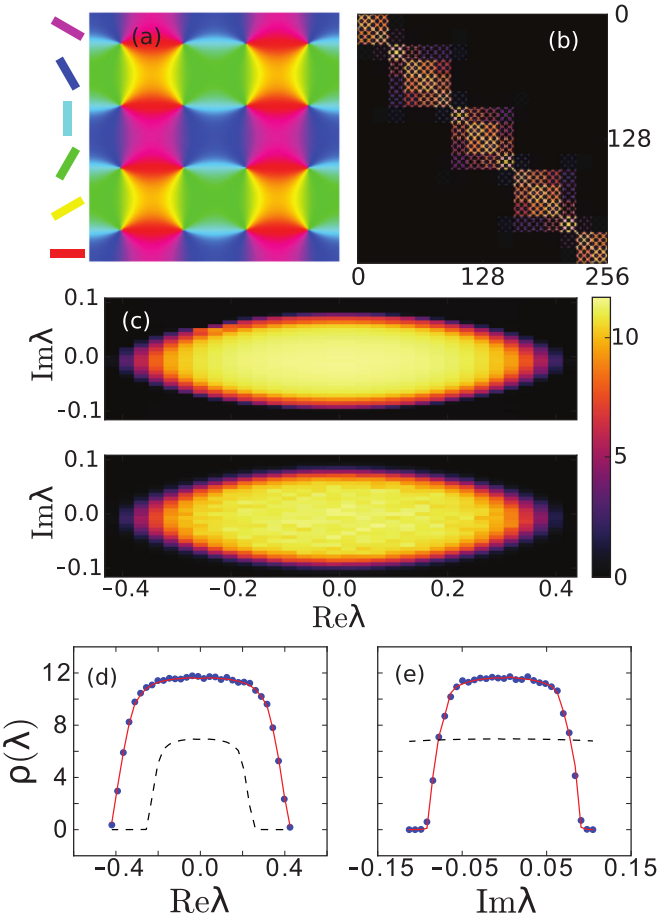

FIG. 3. Analysis of eigenvalue distribution with continuously varying gain (37). (a) Orientation map of neurons. (b) Gain matrix g_{ij}. (c) Eigenvalue density calculated from self-consistent equations (top) and from realizations of J (bottom). Density cross sections along the (d) real and (e) imaginary axes, plotted as in Fig. 2(e).

To verify our results, we consider a network with $M = 3$ populations, with relative population sizes $f = (\frac{1}{6}, \frac{1}{3}, \frac{1}{2})$, and

$$g_{mn}^2 = \begin{bmatrix} 0.54 & 0.83 & 0.65 \\ 0.95 & 0.46 & 0.01 \\ 0.72 & 0.59 & 0.55 \end{bmatrix},$$
$$\tau_{mn} = \begin{bmatrix} 0.5 & -0.2 & 0.9 \\ -0.2 & 0.3 & 0.1 \\ 0.9 & 0.1 & -0.6 \end{bmatrix}. \quad (36)$$

We iteratively solved the self-consistent Eqs. (32) for a grid of points on the complex plane and approximated the eigenvalue distribution using finite differences, shown in Fig. 2(a). We compare this distribution with eigenvalue histograms generated by exact diagonalization of 1000 realizations of J. We find that realizations of J with complex elements agree with our result [Figs. 2(c), 2(e), and 2(f)]. Removing the correlations (4) from realizations of J yields a circular distribution [Fig. 2(b)]. Notably, we find that including these correlations distorts the eigenvalue distribution in a nontrivial way: The distribution is neither a circle nor an ellipse. Furthermore, we find using Eqs. (A4) and (A2) (in the Appendix) that the rightmost eigenvalue of the distribution has moved from $\sim$0.713 to $\sim$0.890, so that the corresponding linear system (1) becomes more unstable.

For any finite N, J has nonuniversal features that disappear as $N \to \infty$. In particular, the matrix J with real elements will have a higher density of eigenvalues on the real axis [Fig. 2(d)]. However, we find that the proportion of eigenvalues on the real axis drops off as $1/\sqrt{N}$, as anticipated for large N [37].

To demonstrate that our technique applies to situations where the variance and covariance depend continuously on the node indices i, j, we consider a neural network inspired by connectivity around pinwheels in the visual cortex [38,39]. The neurons are arranged on a square grid on the unit square and assigned orientations based on their position, shown in Fig. 3(a). For neurons i and j with positions $\mathbf{r}_i$ and $\mathbf{r}_j$, the gain is

$$g_{ij} = g_0 \exp\left[-|\mathbf{r}_i - \mathbf{r}_j|^2/w_r^2 - \Delta\theta^2(\mathbf{r}_i, \mathbf{r}_j)/w_\theta^2 \right], \quad (37)$$

where $\Delta\theta(\mathbf{r}_i, \mathbf{r}_j)$ denotes the difference in orientation of neurons at $\mathbf{r}_i$ and $\mathbf{r}_j$. We choose the covariance to be proportional to the gain: $\tau_{ij} = \tau_0 g_{ij}$. In this example, $w_r = 0.2$, $w_\theta = 20^\circ$, $g_0 = 1$, and $\tau_0 = 0.8$. The gain matrix for a grid of 16×16 neuron populations is shown in Fig 3(b). This grid

size requires us to solve $N = 256$ self-consistent equations to determine the eigenvalue density. For comparison, we generated 1000 realizations of J with $N = 2048$; to mitigate finite-N effects [4], we used block structured matrices with 16×16 populations, with eight nodes in each population. We find that our result closely matches the empirical distribution [Figs. 3(c)–3(e)]. Increasing the grid size to 32×32 and 64×64 did not appreciably change the resulting eigenvalue distribution, indicating that the current resolution is sufficient. Finally, using Eqs. (29) and (30), we find that including correlations moves the rightmost eigenvalue from 0.24 to 0.41, decreasing the stability of the system.

Our results can be extended to more general correlation structures, such as correlations between arbitrary blocks or clusters. However, including more general correlations increases the number of self-consistent equations that must be solved in (16). Our results can also be extended to the case of nonzero mean as in Ref. [33]. The diagrammatic technique can also be used to study further quantities of interest such as eigenvalue correlations [30], eigenvector correlations [40,41], and linear dynamics not captured by the eigenvalues [33].

In conclusion, we have adapted the diagrammatic technique to study correlated connectivity matrices that are not independently or identically distributed, and relevant to biological circuits. The results indicate that the presence of correlations can dramatically influence the network stability and dynamics. The correlation structure is determined by plasticity rules, which act locally on connections between nodes [16,18]. The presented analytical framework therefore makes it possible to evaluate the impact of local plasticity rules on global network activity.

This research was supported by NSF CAREER Award No. IIS-1254123 and NSF Grant No. IOS-1556388, as well as NEI Grants No. P30 EY019005 and No. T32 EY020503 and the Salk Institute Innovations Grant Program. The authors thank Nicolas Brunel for discussions.

APPENDIX

Derivation of the boundary of the eigenvalue distribution in the absence of covariance between matrix elements. Here we first show that the eigenvalue density (26) for J with independent elements ($\tau_{ij} = 0$) has support on the disk with radius $R = \sqrt{\lambda_1(K)}$, where $\lambda_1(K)$ is the largest eigenvalue of the matrix $K_{ij} \equiv g_{ij}^2/N$. There are two solutions to the self-consistent equations (24) in the limit $\epsilon \to 0$: a trivial solution, with all $a_i = d_i = 0$, and a nontrivial solution, with all $a_i, d_i > 0$ [42]. The trivial solution corresponds to the region where $\rho(r) = 0$ [27,31]. Indeed, we see that when $a_i = d_i = 0$, all $q_i = r^2$. Then, by (24), $c_i = 1/z$, and therefore $\rho(r) = 0$ by (26).

Now consider the region where $\rho \neq 0$, where all the a_i and d_i are nonzero. Then, combining (24) and (25) for d_i in the $\epsilon \to 0$ limit yields

$$q_i d_i = \frac{1}{N} \sum_j g_{ij} d_j. \tag{A1}$$

We determine the radius R of the boundary by finding where the two solutions match. Assuming continuity of the a_i and d_i, then as $d_i \to 0^+$ as we approach the boundary, all the $q_i \to R^2$. Then, in the limit, (A1) indicates that d is an eigenvector of $K_{ij} = g_{ij}^2/N$ with eigenvalue R^2. Furthermore, since K and d have only positive entries, R^2 must be the largest eigenvalue $\lambda_1(K)$ of K by the Perron-Frobenius theorem. Thus, the boundary of the eigenvalue distribution has radius $R = \sqrt{\lambda_1(K)}$. A nearly identical argument shows $K_{mn} = g_{mn}^2 f_n$ for the block structured case. This result was previously presented in Refs. [43] and [4], and a similar argument was used in Ref. [33] for the case of matrices with nonzero mean. However, previous analyses do not hold when J has covariant elements.

Boundary with covariance. Now we show that when $\tau_{ij} \neq 0$, the boundary of the eigenvalue distribution satisfies (29) and (30). Again, we have $a_i, d_i \neq 0$ on the support of the eigenvalue distribution, and $a_i = d_i = 0$ otherwise. Plugging the trivial solution into (27), the c_i now satisfy

$$c_i = \left(z - \sum_j \tau_{ij} g_{ij} g_{ji} c_j \right)^{-1}. \tag{A2}$$

Now, approaching the boundary from the inside as before, in the limit $d_i \to 0^+$,

$$d_i = \sum_j |c_i|^2 g_{ij}^2 d_j, \tag{A3}$$

where the c_i satisfy (A2) in the limit. Since all the $d_i > 0$, this means that d is the Perron-Frobenius eigenvector of the matrix $K_{ij} = |c_i|^2 g_{ij}^2$ with eigenvalue 1. This means that the points z on the boundary satisfy

$$\lambda_1(K) = 1, \tag{A4}$$

where $\lambda_1(K)$ is the largest modulus eigenvalue of K. Together, (A2) and (A4) determine the points z that lie on the boundary of the eigenvalue distribution. We have found that these equations can be solved efficiently as follows: First we write $z = re^{i\theta}$ and fix θ. Then, to find the r satisfying (A4), we use a root finding algorithm: At each step of the root finding algorithm, we iterate (A2) to find the $c_i(z)$.

If g_{ij} is block structured, then we have only M variables c_m, with

$$c_m = \left(z - \sum_n \tau_{mn} g_{mn} g_{nm} f_n c_n \right)^{-1} \tag{A5}$$

and

$$K_{mn} = |c_m|^2 g_{mn}^2 f_n. \tag{A6}$$

[1] H. Sompolinsky, A. Crisanti, and H. J. Sommers, Phys. Rev. Lett. **61**, 259 (1988).

[2] K. Rajan and L. F. Abbott, Phys. Rev. Lett. **97**, 188104 (2006).

[3] J. Aljadeff, M. Stern, and T. Sharpee, Phys. Rev. Lett. **114**, 088101 (2015).
[4] J. Aljadeff, D. Renfrew, M. Vegué, and T. O. Sharpee, Phys. Rev. E **93**, 022302 (2016).
[5] M. Aldana, E. Balleza, S. Kauffman, and O. Resendiz, J. Theor. Biol. **245**, 433 (2007).
[6] R. M. May, Nature (London) **238**, 413 (1972).
[7] S. Allesina, J. Grilli, G. Barabás, S. Tang, J. Aljadeff, and A. Maritan, Nat. Commun. **6**, 7842 (2015).
[8] E. P. Wigner, Ann. Math. **67**, 325 (1958).
[9] P. W. Anderson, Phys. Rev. **109**, 1492 (1958).
[10] H. Sompolinsky and A. Zippelius, Phys. Rev. B **25**, 6860 (1982).
[11] S. N. Majumdar and M. Vergassola, Phys. Rev. Lett. **102**, 060601 (2009).
[12] E. J. Candes and T. Tao, IEEE Trans. Inf. Theory **52**, 5406 (2006).
[13] D. Sussillo and L. F. Abbott, Neuron **63**, 544 (2009).
[14] N. Bertschinger and T. Natschläger, Neural Comput. **16**, 1413 (2004).
[15] K. Rajan, L. F. Abbott, and H. Sompolinsky, Phys. Rev. E **82**, 011903 (2010).
[16] M. Gilson, A. N. Burkitt, D. B. Grayden, D. A. Thomas, and J. L. van Hemmen, Biol. Cybern. **101**, 427 (2009).
[17] S. Song, P. J. Sjöström, M. Reigl, S. Nelson, and D. B. Chklovskii, PLoS Biol. **3**, e68 (2005).
[18] D. Miner and J. Triesch, PLoS Comput. Biol. **12**, e1004759 (2016).
[19] Vinayak and A. Pandey, Phys. Rev. E **81**, 036202 (2010).
[20] P. Shukla, Phys. Rev. E **71**, 026226 (2005).
[21] A. Khorunzhii, Math. Fiz. Anal. Geom. **3**, 80 (1996).
[22] Z. Burda, J. Jurkiewicz, and B. Wacław, Phys. Rev. E **71**, 026111 (2005).
[23] H. J. Sommers, A. Crisanti, H. Sompolinsky, and Y. Stein, Phys. Rev. Lett. **60**, 1895 (1988).
[24] J. Grilli, T. Rogers, and S. Allesina, Nat. Commun. **7**, 12031 (2016).
[25] This relation follows from the solution $\bar{\partial}\partial \log z = \pi\delta(x)\delta(y)$ of Poisson's equation in two dimensions. See also Ref. [27].
[26] J. Ginibre, J. Math. Phys. **6**, 440 (1965).
[27] J. Feinberg and A. Zee, Nucl. Phys. B **504**, 579 (1997).
[28] E. Brézin, C. Itzykson, G. Parisi, and J.-B. Zuber, Commun. Math. Phys. **59**, 35 (1978).
[29] E. Brézin and A. Zee, Phys. Rev. E **49**, 2588 (1994).
[30] R. A. Janik, M. A. Nowak, G. Papp, and I. Zahed, Nucl. Phys. B **501**, 603 (1997).
[31] J. Feinberg, J. Phys. A: Math. Gen. **39**, 10029 (2006).
[32] G.' t Hooft, Nucl. Phys. B **72**, 461 (1973).
[33] Y. Ahmadian, F. Fumarola, and K. D. Miller, Phys. Rev. E **91**, 012820 (2015).
[34] It is worth noting that since the correlators (3) and (4) are not proportional to the identity as in the independently and identically distributed (i.i.d.) case, loops produce a weighted trace weighted by elements of g_{ij}. However, assuming all elements of g_{ij} are of $O(1)$, the weighted trace is of $O(N)$ as in the i.i.d. case.
[35] We furthermore demand that g_{ij} converges to a uniformly bounded continuous function $g(i/N, j/N)$ on the unit square as $N \to \infty$, excepting discontinuities on a set of measure zero (see Ref. [4]).
[36] These sums converge, since the Green's function for H, $\frac{1}{N}\mathrm{tr}\,\mathcal{G} = \sum_i (A_{ii} + D_{ii})$ and Eq. (28) must converge.
[37] A. Edelman, E. Kostlan, and M. Shub, J. Am. Math. Soc. **7**, 247 (1994).
[38] B. K. Murphy and K. D. Miller, Neuron **61**, 635 (2009).
[39] F. Wolf, Phys. Rev. Lett. **95**, 208701 (2005).
[40] J. T. Chalker and B. Mehlig, Phys. Rev. Lett. **81**, 3367 (1998).
[41] R. A. Janik, W. Nörenberg, M. A. Nowak, G. Papp, and I. Zahed, Phys. Rev. E **60**, 2699 (1999).
[42] It is not hard to show that if just one a_i or d_i is zero, all are zero.
[43] J. Aljadeff, D. Renfrew, and M. Stern, J. Math. Phys. **56**, 103502 (2015).